Influence of adhesion and friction on the geometry of packings of spherical particles

C. L. Martin*
INP Grenoble, SIMAP GPM2, CNRS UMR5266, UJF, ENSPG, Boîte postale 46, 38402 Saint Martin d'Hères cedex, France

R. K. Bordia
Department of Materials Science and Engineering, University of Washington, Box 352120, Seattle, Washington 98105, USA
(Received 24 May 2007; revised manuscript received 18 October 2007; published 18 March 2008)

We study the effect of both adhesion and friction on the geometry of monosized packings of spheres by means of discrete element simulations. We use elastic properties that are characteristic of materials typically used for particulate processing (Young's modulus in the range 20–200 GPa). The geometrical features, both global and local, of the packings are studied using a variety of approaches in order to investigate their ability to quantify the effect of adhesion and/or friction. We show that both adhesion and friction interaction decrease the packing fraction. The very localized ordering that adhesion triggers is particularly investigated by use of the radial distribution function, the ordering parameter Q_6, and four triclinic cells that allow a description of the microstructure at the local level. We show that the probability of occurrence of these triclinic cells is approximately proportional to their degree of freedom when neither adhesion nor friction plays a role. We find that the introduction of adhesive interactions increases the probability of occurrence of those cells that have the lowest degree of freedom.

DOI: 10.1103/PhysRevE.77.031307 PACS number(s): 45.70.−n, 61.43.Gt, 45.70.Cc, 45.50.−j

I. INTRODUCTION

Random packings of spherical particles are useful models of simple liquids, metallic glasses, granular materials, and engineering powders [1–3]. The highly complex topological features associated with disorder in such systems can be described in simple geometric terms, through the radius and position of each sphere. Much progress has been made in the last 20 years in the study of such random packings with particular attention to random close packings (RCPs). The quantification of the degree of order (or disorder) in such packings has led to the questioning of the validity of the RCP definition because its packing fraction depends on the preparation protocol [4]. Also, the concepts of randomness and close packing are somewhat contradictory when these packings are built. Indeed, it appears that there exists a trade-off between the packing fraction and order since an amorphous packing can be made slightly more dense by introducing small amounts of crystallinity [5–10]. In this context, the better-defined concept of the maximally random jammed state has been introduced [7]. Detailed studies have also been carried out on the geometric features that characterize dense packings [11].

The above numerical studies deal with ideal packings of hard spheres that are good model systems for studying liquid-solid phase transitions. This paper is more concerned with the properties of real granular packings. Granular materials differ from frictionless and nonadhesive sphere packings and their physical properties may not be deduced simply from hard sphere systems. The behavior of such dense and dilute granular media has been simulated with applications in various fields of science and engineering [12–15]. In these simulations, interparticle friction is removed to prepare dense samples, and adhesion is not introduced. The aim of this work is to use the tools developed for studying ideal systems to gain more insight into the structure of real granular packings by incorporating adhesive and frictional forces in computer simulations during the preparation stage. These two effects are key to generating realistic granular packings.

Friction effects alone have been introduced to investigate, in particular, how the coordination number decreases from $z=6$ as friction increases [15]. On the other hand, adhesive forces become non-negligible for sufficiently small or sufficiently compliant particles and play an important role in the numerous powder processes for which particle size is under 10 μm [16]. Discrete simulations on cohesive powders have been reported recently in two dimensions (2D) [17], and 3D simulations were also conducted for packings of very soft fine particles (Young's modulus $E=0.01$ GPa) with long-range cohesive forces of van der Waals type under gravity [18,19]. In any case, these numerical studies lead to highly porous packings that collapse under small pressure [20]. It is not clear if the resulting packings retain some signature of the adhesive and frictional forces that are present at the contact level.

We thus introduce both friction and adhesive forces in order to model realistic 3D granular systems that are subjected to small pressures. Practitioners define the packing density of such packings as the tap density and consider this microstructure as the starting one, prior to compaction or sintering. Hence, we study the specific geometrical features that adhesive and frictional forces bring to these dense packings. In particular, we show that the tensile adhesive forces that act at the contact level between particles generate peculiar geometric features that have not been reported earlier. Although we focus on particles with elastic properties that are characteristics of hard polymers (Young's modulus $E=20$ GPa), we have also studied particles with higher elastic properties ($E=200$ GPa) that are more representative of ceramics.

*Christophe.Martin@simap.grenoble-inp.fr

TABLE I. Material parameters.

Young's modulus E	Poisson's coefficient ν	Surface energy γ	Friction coefficient	Particle size
20–200 GPa	0.3	0.0–1.0 J m^{-2}	0.0–0.2	1 μm

II. GENERATION OF SPHERE PACKINGS WITH ADHESION AND FRICTION

We rely on discrete element simulations to generate a representative set of packings made of 1000–8000 identical spheres of radius R in a simulation box [21]. Periodic boundary conditions are used on all three axes such that, when a particle protrudes outside the periodic cell through a given face, it interacts with the particles on the opposite face. Particles are treated as deformable (although very stiff) elastic spheres $\left(E^*=\frac{E}{2(1-\nu^2)}\right)$. The introduction of adhesion (work of adhesion $w=2\gamma$ with γ the surface energy) may be accounted for by the Johnson-Kendall-Roberts (JKR) model [22] or the Derjaguin-Muller-Toporov (DMT) model [23], which apply to opposite ends of the spectrum of contact behavior. The limit of validity of each model is given by Tabor's parameter [24]

$$\mu \equiv \left(\frac{R^* w^2}{E^{*2} z_0^3}\right)^{1/3}, \tag{1}$$

where z_0 is the range of surface forces and $R^*=R/2$ is the contact equivalent radius. The DMT theory is more appropriate for low values of μ ("small hard" particles) while the JKR theory applies to large values of μ ("large compliant" particles). However, it has been shown that the JKR equations are valid in conditions well outside the expected JKR zone [25,26] while the DMT condition of a large cohesive zone size is met only for very stiff nanoscale contacts [16]. The exact value of z_0 is difficult to ascertain but taken generally as one atomic radius [25]. The material parameters used in the simulations (see Table I) may lead to either the JKR or DMT limits (or to cases in between). We have thus implemented both models to study their impact on our results.

Depending on the model used, the normal force N is given by the DMT or JKR equation:

$$N^{\mathrm{JKR}} = \frac{4E^* a^3}{3R^*} - 2\sqrt{2\pi w E^* a^3},$$

$$N^{\mathrm{DMT}} = \frac{4E^* a^3}{3R^*} - 2\pi w R^*, \tag{2}$$

where a is the contact radius. The Hertz theory leads to the exact value of a for the DMT model while it is only an approximation in the JKR model:

$$a^2 = R^* h, \tag{3}$$

where h is the indentation between the two particles.

Tensile forces are thus included in the model and decohesion occurs for the pull-off force N_c:

$$N_c^{\mathrm{JKR}} = -\frac{3}{2}\pi w R^*,$$

$$N_c^{\mathrm{DMT}} = -2\pi w R^*. \tag{4}$$

The tangential force model is of the Hertz-Mindlin type in the sticking mode, while the norm of the tangential force is limited during sliding by Coulomb friction (friction coefficient μ). Rotations are fully included in the simulations while no rotational resistance is introduced. Material parameters chosen for the present simulations are summarized in Table I. Effective surface energy and particle size have been chosen such that adhesive forces play a significant although realistic role in the packing.

The procedure for obtaining random jammed packing consist in first generating a gas of nonoverlapping spheres located at random positions in the periodic simulation box. This leads to an initial packing fraction $\phi=0.32$. The packing is then subjected to a stress-controlled hydrostatic densification. Contact forces appear in the box and kinetic energy is dissipated by viscous forces that are introduced at the contact level. The macroscopic pressure P is calculated from Love's formulation [27]. Starting from $\dot{\Gamma}_0=10^{-4}$ s^{-1}, the hydrostatic densification rate $\dot{\Gamma}$ is calculated, as densification proceeds, with a simple proportional controller [13]

$$\dot{\Gamma} \propto \dot{\Gamma}_0 \frac{P_c - P}{P_c}, \tag{5}$$

where P_c is the control pressure. Note that the simulation box may expand if $P>P_c$. With such a scheme, a maximum packing fraction is asymptotically approached while the pressure tends toward the control pressure, which has been chosen to be small in comparison to the material properties ($P_c=0.02$ MPa has been used here). In particular, the ratio $P_c R^2/|N_c|$ is small in our simulations (<0.025) [17].

The densification scheme described above allows particles to overlap each other to generate contact forces. When adhesion is not included for softer particles ($E=20$ GPa), the maximum normalized overlap between particles, $h/2R$, is less than 5×10^{-4} with $P_c=0.02$ MPa. Stiffer particles ($E=200$ GPa) lead to smaller overlaps ($h/2R<10^{-4}$). When adhesion is included, the indentation is of course much larger due to the tensile nature of adhesive forces. In that case, we observed $h/2R$ to be in the range $0.02<h/2R<0.025$ for the softer material.

III. PACKING CHARACTERISTICS

Four different cases have been investigated depending on the presence of adhesion and/or friction. Each case has been treated with both the JKR and the DMT models. The typical evolution of the densification rates is illustrated in Fig. 1 for these various cases for the softer material with the JKR model. The densification process is stopped when the densification rate attains very low values ($\dot{\Gamma}<10^{-6}\dot{\Gamma}_0$). At this point, we consider that further densification is prevented by the jamming of the particle assembly. We observed that the

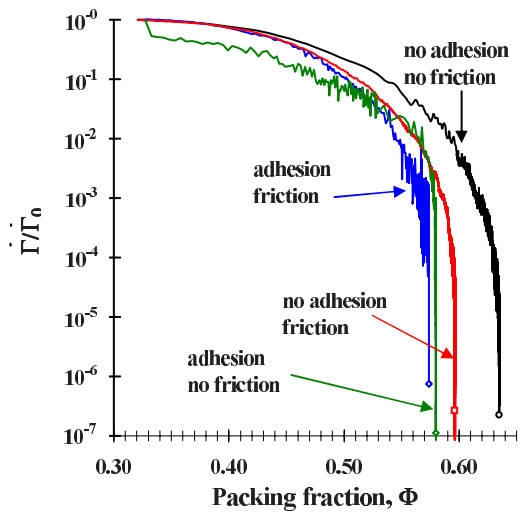

FIG. 1. (Color online) Evolution of the densification rate for four different packings with the softer elastic properties ($E=20$ GPa) and the JKR contact model. The densification protocol is given by Eq. (5) with a control macroscopic pressure $P_c=0.02$ MPa.

maximum packing fraction attained with this algorithm does not depend on the size of the system for packings made of more than 1000 spheres (using periodic conditions). Whatever the type of interaction, a few particles with fewer than four contacts were observed (from 1% to 7%). We also checked that, apart from these rattler particles, all other particles cannot be displaced without generating an increase in contact forces with neighboring particles. This property qualifies the packings as *locally jammed* as defined by Torquato and Stillinger [28]. We further checked that the net forces F on nonrattler particles are very small, thus leading to quasistatic equilibrium ($F<10^{-4}P_c$).

Each condition was repeated at least five times with different initial random seeds for the generation of the initial gas of particles for the softer material. The four conditions for the packings with the particles with the highest Young's modulus ($E=200$ GPa) were tested only once per adhesive contact model (JKR and DMT). This is because the stiffer particles lead to much larger CPU times (smaller time step) that do not allow for such duplications (thus we are not able to give error estimates for these stiff particle packings). In the remainder of the paper, unless stated otherwise, all simulation results relate to the softer material parameters ($E=20$ GPa).

The average packing fraction of packings densified with neither adhesive nor friction forces is $\Phi=0.6349$. This value is close to the value of the traditionally termed *random close packed* state. The coordination number of these packings is 6.04. Here we define the coordination number as the number of contacts per particle that transmit force (true geometrical contact).

Figure 1 indicates clearly that, under our protocol, friction forces decrease the maximum attainable packing fraction. The average packing fraction is $\Phi=0.598$ for packings prepared with a friction coefficient of 0.2 and no adhesion. We have observed that friction decreases the mean coordination number as compared to packings without friction (see Table II). This is in agreement with other results on elastic packings that show that friction acts primarily as a kinematic constraint [13,29]. A larger friction coefficient is associated with a reduced number of contacts required to achieve a stable configuration [29,30]. However, the introduction of a limited friction (here $\mu=0.2$) does not lead to the theoretical limit of four contacts. We have tested larger friction coefficients (up to $\mu=0.5$) and found, in accordance with Silbert *et al.* [15] and Yang *et al.* [19], that increasing the friction coefficient leads to only a gradual decrease of the coordination number.

Adhesion also decreases the maximum attainable packing fraction. However, when friction is not included, it is associated with a larger coordination number caused by tensile adhesive forces (between 6.07 and 6.11 depending on the contact model for adhesion). Adhesion generates denser clusters of particles that are difficult to break apart due to the tensile force involved [Eq. (4)]. These clusters hinder rearrangements, thus lowering the final packing fraction. The characteristics of these clusters will be studied in the following sections.

Packings with adhesion and friction have approximately the same maximum packing fraction as packings with adhesion only. However, the coordination number associated with these packings is lower than the coordination number of the packings with adhesion only. For these packings, friction and adhesion have opposite effects on the mean coordination

TABLE II. Characteristics of packings with JKR and DMT adhesive models.

	Surface energy γ (J m^{-2})	Friction coefficient μ	Packing fraction Φ JKR	Packing fraction Φ DMT	Coordination number Z JKR	Coordination number Z DMT
$E=20$ GPa	0.0	0.0	0.6349 ± 0.0004		6.04 ± 0.02	
(five packings)	0.0	0.2	0.598 ± 0.002		5.36 ± 0.02	
	1.0	0.0	0.579 ± 0.002	0.570 ± 0.002	6.11 ± 0.03	6.07 ± 0.01
	1.0	0.2	0.574 ± 0.005	0.564 ± 0.002	5.8 ± 0.1	5.9 ± 0.1
$E=200$ GPa	0.0	0.0	0.631		5.90	
(one packing)	0.0	0.2	0.597		5.22	
	1.0	0.0	0.572	0.563	6.13	6.03
	1.0	0.2	0.569	0.558	6.09	5.98

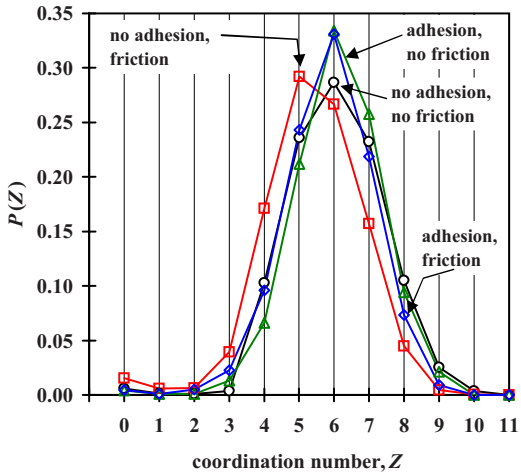

FIG. 2. (Color online) Probability distribution of the coordination number for the four packings described in Fig. 1.

number, resulting in coordination characteristics that share some aspects of adhesive-only and friction-only packings.

Increasing the stiffness of the particles from 20 to 200 GPa consistently decreases the packing fraction by a small amount as shown in Table II. The coordination number is also somewhat decreased for the case where adhesion is not introduced. However, it is interesting to note that adhesion increases the coordination number of stiff particles at least as much as it does for softer particles. Generally, it is believed that adhesion affects only soft small particles [16,25]. Here we show that the packings made of small stiff particles such as ceramics may also be affected by adhesion.

The effect of the adhesive model (JKR or DMT) can be seen in Table II. The DMT model consistently leads to a slightly lower packing fraction. This may be understood by inspection of Eq. (4), which shows that the pull-off force in the DMT model is slightly larger (by a 4/3 factor) than the JKR pull-off force. Clusters of particles are thus somewhat less prone to rearrangements in the DMT model. In any case, although these two models apply to opposite ends of the adhesive contact behavior, they lead to very similar macroscopic packings. In the remainder of the paper, unless stated otherwise, we have chosen to show simulation results from the JKR model only since the two models lead to the same qualitative results.

Figure 2 shows the distribution of coordination numbers for the four types of packing studied here with $E=20$ GPa and the JKR model. The distributions exhibit a Gaussian shape when the particles with low coordination number are excluded ($Z<4$). Although the four packings show the same type of distribution, important differences arise depending on the introduction of friction and/or adhesion. Friction translates the peak of $P(Z)$ toward smaller coordination values (at $Z=5$ instead of 6). Also, friction enables a larger number of rattlers ($Z<3$, 7% instead of 1%) to remain. Conversely, the introduction of adhesion shifts the distribution toward larger coordination numbers. However, adhesion does not inhibit rattlers, nor does it promote the appearance of particles with a very large number of contacts ($Z>10$) which would indicate some crystallization. Finally, it should be clear that, because gravity is not introduced in these simulations, the probability distribution of the case with friction and no adhesion may not reflect realistically the case of large particles with friction.

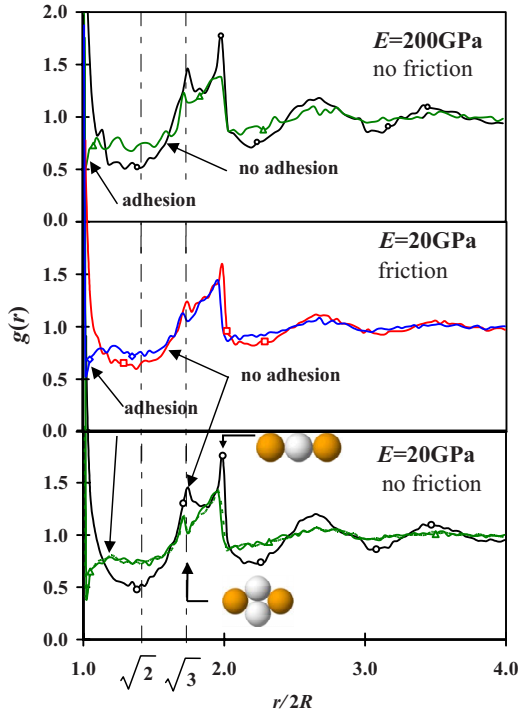

FIG. 3. (Color online) Radial distribution function for the four packings whose densification is described in Fig. 1. The contributions of certain motifs to $g(r)$ are indicated. Bottom, packings without friction, $E=20$ GPa; ○, no adhesion; △, adhesion. The dotted curve relates to the DMT adhesive model; all other curves with adhesion are obtained with the JKR model. Middle, packings with friction $E=20$ GPa; □, no adhesion; ◇, adhesion. Top, same as bottom figure for the stiffer particles ($E=200$ GPa).

IV. RADIAL DISTRIBUTION FUNCTION

In order to gain some more insight into the microstructure of the packings generated in the previous section, we first consider the radial distribution function $g(r)$ (or pair-correlation function) which may indicate structural changes when small shoulders or maxima appear [31]. Also, $g(r)$ gives information about long-range interparticle correlations and their organization. Figure 3 shows the $g(r)$ functions for the various packings studied here.

The $g(r)$ curve associated with the packings without adhesion or friction is very similar to those reported earlier on 3D numerical packings [7,10,18] or on real packings observed by x-ray tomography [32]. Note, in particular, the two typical peaks at $r/2R=\sqrt{3}$ and 2 which relate to specific configurations and the abrupt decrease after the $r/2R=2$ peak. Also, note the absence of any peak at $r/2R=\sqrt{2}$ and $\sqrt{5}\approx 2.236$, which would indicate a crystallization of the packing.

The $g(r)$ curve that characterizes the packings that have been prepared with adhesion and no friction also exhibits

two peaks around $r/2R=\sqrt{3}$ and 2 but of a smaller amplitude and the peaks are translated to smaller values (1.71 and 1.96, respectively). The translation to lower $r/2R$ values is, of course, due to the increased indentation that characterize adhesive particles ($0.02<h/2R<0.025$ with the material data of Table I). Adhesion does not bring detectable crystallization as shown by the absence of a peak at $r/2R=\sqrt{2}$ or $\sqrt{5}$.

The most striking feature of this curve arises in the vicinity of the true contact ($r/2R>1$) where a deep well exists. This well is linked to the larger coordination number that characterizes the adhesive packings (6.07 to 6.11 contacts per particle depending on the adhesive model) as compared to the nonadhesive ones (6.04). Adhesive particles that happen to be close to each other will stick together after a collision and form a true contact which is more likely to survive further densification, thus depleting the immediate $r/2R>1$ domain. Accordingly, we also observed a well in the distribution of contact pair angles in the vicinity of $\pi/3$. It should be clear that this well is not due to the increased value of the indentation for adhesive particles but is due to the tensile nature of adhesion forces. A similar well was observed on the radial distribution function for highly porous packings of fine adhesive particles [18] and for colloids with Baxter's adhesive hard sphere model [33].

The main features of the two $g(r)$ curves associated with the packings prepared with friction are similar to those associated with the packings prepared without friction. However, the peaks for the packings with friction only are less marked as reported in [15]. The well close to $r/2R=1$ that characterizes adhesive packings is also less marked when friction is introduced.

We have observed that stiffer particle packings exhibit very similar $g(r)$ curves as compared to the softer ones. For example, Fig. 3 shows that the packings made of stiff or soft particles exhibit the same characteristic features. In particular, the well in the vicinity of the true contact appears nearly as sharply for the stiff adhesive particles. Hence, in the range of Young's modulus (20–200 GPa) that we have studied, the packing characteristics do not depend on the stiffness of the particles.

Also, we have verified that the adhesive contact model does not play any significant role in the $g(r)$ curves associated with the packings prepared with adhesion (see dotted curve in bottom panel of Fig. 3).

V. BOND-ORIENTATIONAL ORDER Q_6

The preceding section has shown that the introduction of adhesion modifies quite drastically the radial distribution function of jammed packings. In this section, we investigate the effect of adhesion and friction on the crystallinity of the prepared packings. We use the bond-orientational order metric Q_6 defined by Steinhardt, Nelson, and Ronchetti [34] based on the spherical harmonics $Y_{6m}(\theta,\varphi)$:

$$Q_6=\left(\frac{4\pi}{13}\sum_{m=-6}^{6}\langle Y_{6m}(\theta,\varphi)\rangle^2\right)^{1/2}, \qquad (6)$$

where θ_k and ϕ_k are the polar and azimuthal angles of bond k. Here, a bond is defined as a true contact transmitting force.

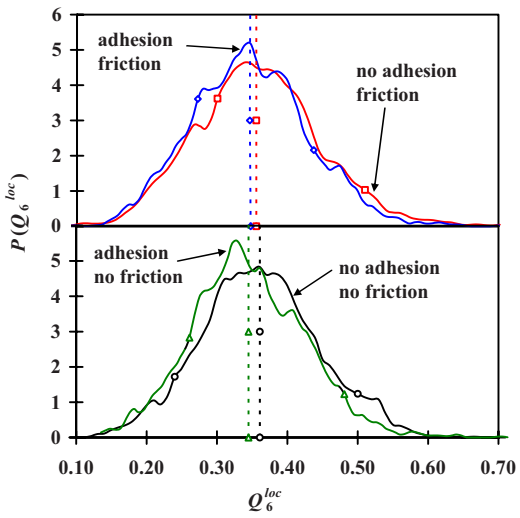

FIG. 4. (Color online) Distribution of Q_6^{local} with and without adhesion. Straight broken lines give averages. Bottom, packings without friction, △, ○. Top, packings with friction, □, ◇.

We have relaxed this bond definition to include nearest neighbors that are not truly in contact [up to $1.2(2R)$] without observing significant differences in the value of Q_6. Averaging in Eq. (6) may be performed over all bonds. In that case, it represents the *global* measure of crystallization (Q_6^{global}) and tends to zero for disordered packings. Q_6^{global} reaches its maximum for a fcc lattice at 0.574 52. If the averaging in Eq. (6) is performed for each particle, it represents the *local* measure of order (Q_6^{local}).

The values of Q_6^{global} for all our packings are very small (<0.1), whatever the adhesion and friction conditions. Furthermore, no noticeable difference was observed between the four types of packings studied here.

We then turn our attention to Q_6^{local} that should be more appropriate to detect local measure of order in our packings. Figure 4 shows the distribution of Q_6^{local} for the four types of packing. Curves for the nonadhesive particles show a Gaussian shape. The shape and average values of these distribu-

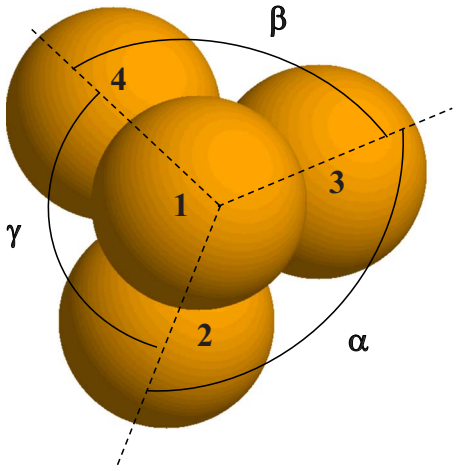

FIG. 5. (Color online) Four particles forming a triclinic cell with angles ($\phi=0.635$) (α,β,γ).

tions are very similar to those already observed for noncrystallized packings [8,10]. One may observe that the curves relating to the adhesive packings exhibit a sharper maximum with shoulders on both sides. The most noticeable feature of the curve related to adhesive packings is its asymmetry as compared to nonadhesive packings. It is difficult to ascribe a clear significance to these features.

The calculation of the Q_6^{local} distribution is not able to discriminate clearly the effect of adhesion on the structure of packings. This means that the very local ordering that may come with the introduction of adhesion is not sufficient to trigger higher values of Q_6^{local}. Other tools like the radial distribution function $g(r)$ described in the preceding section are better suited for describing the effect of adhesive forces.

VI. TRICLINIC CELLS

We seek to characterize more precisely the above generated jammed packings by defining various primitive geometric cells or geometric motifs that give more useful information on the microstructure than the radial distribution function and the Q_6 order measures. In 3D, these primitive unit cells are triclinic and are characterized by three angles α, β, and γ (Fig. 5). The solid volume of each cell is equal to the volume of a sphere. Using the approach presented in [35], we define four subsets of possible cells depending on the values of the triplet (α,β,γ).

The first primitive cell is the densest and characterizes a face centered cubic packing (fcc). In that case all three angles are equal to $\frac{\pi}{3}$ and no further densification of the cell is possible, i.e., any motion of the spheres in the cell will lead to dilation. We define this cell as having no degree of freedom for further packing.

The second subset relaxes one angle. For example, $(\frac{\pi}{3}<\alpha\leq\frac{\pi}{2},\ \beta=\frac{\pi}{3},\ \gamma=\frac{\pi}{3})$ leads to the loss of the contact between spheres 2 and 3 but keeps two sets of planes close packed. The densification of this primitive cell is possible only by decreasing α, thus leading to a primitive cell with one degree of freedom.

The third subset relaxes two angles. For example, $(\frac{\pi}{3}<\alpha\leq\frac{\pi}{2},\ \frac{\pi}{3}<\beta\leq\frac{\pi}{2},\ \gamma=\frac{\pi}{3})$ leads to the loss of the contact between spheres 2 and 3 and between spheres 3 and 4 and keeps only one plane close packed. This primitive cell has two degrees of freedom for further packing.

The fourth cell relaxes all three angles and leaves no close packed plane. This cell has three degrees of freedom for further packing. Note that we include in the definition of this fourth cell those which only form cells with one or more angles that are smaller than $\frac{\pi}{2}$. Typically, rattlers are part of this fourth type of cell.

Figure 6 illustrates the existence of fcc type of cells for various packings (white particles pertain to a fcc cell). Clearly, adhesion triggers the appearance of a number of localized fcc cells [Fig. 6(b)]. Such cells are approximately five times more likely with adhesion as compared to the case without adhesion. The packing prepared with friction exhibited very few fcc cells as illustrated in Fig. 6(c), for which only one fcc cell is seen.

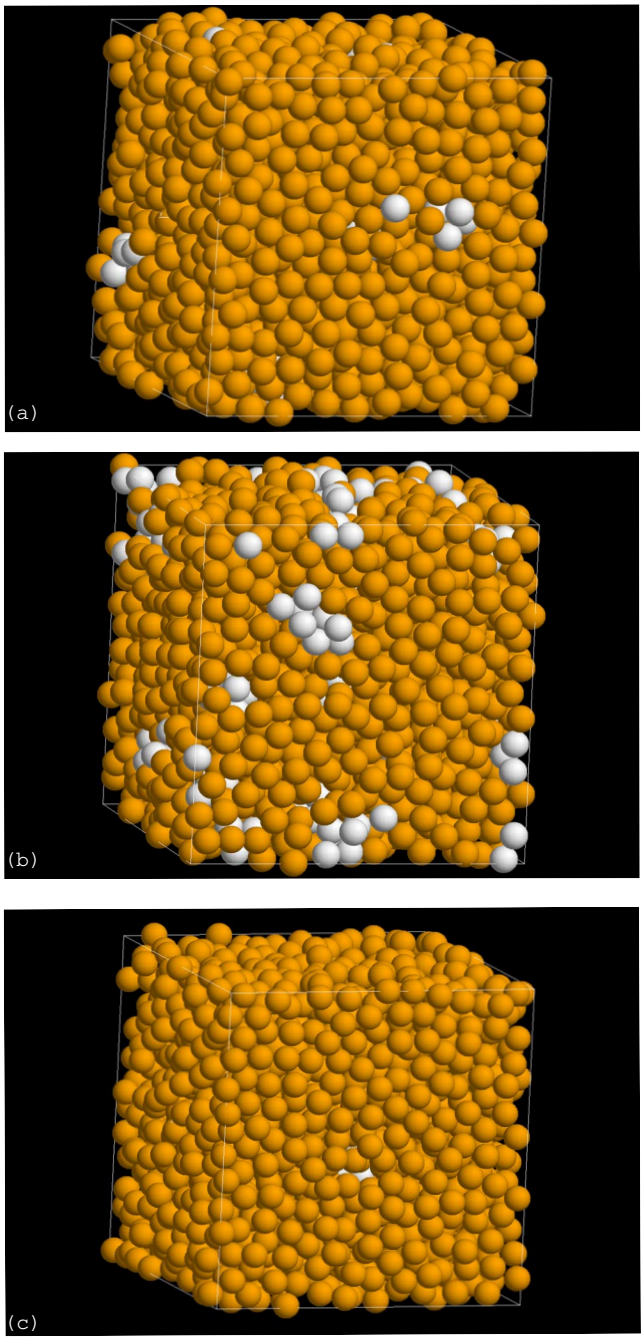

FIG. 6. (Color online) Three packings with 2000 particles, periodic conditions. White particles pertain to a triclinic cell of fcc type. (a) Packing without adhesion or friction. (b) Packing with adhesion and no friction (ϕ=0.579). (c) Packing without adhesion and with friction (ϕ=0.598).

The probability of occurrence x_i of the four types of cell that have been defined above has been calculated. Figure 7 shows these probabilities as a function of the degree of freedom of each cell. Error bars have been included to take into account the five simulations carried out for each type of packing. The line that gives a linear relation between x_i and the degree of freedom is also shown in Fig. 7 for comparison $(x_i=0/6,\ 1/6,\ 2/6,\ 3/6)$.

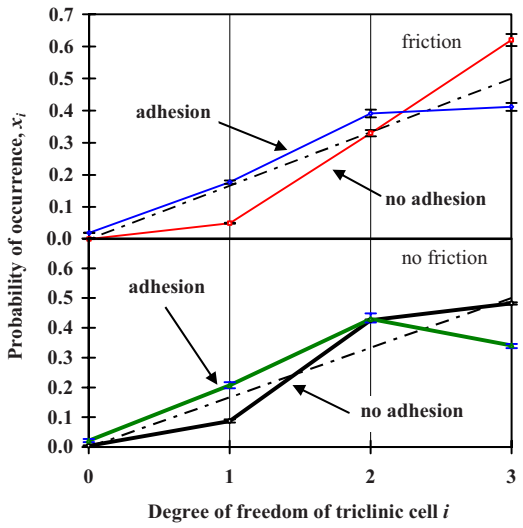

FIG. 7. (Color online) Probability distribution of the four triclinic cells for packings with and without adhesion. The line (- - -) assumes that x_i is proportional to the degree of freedom of the cell [35]. Bottom, packings without friction, △, ○. Top, packings with friction, □, ◇.

Not surprisingly, the packing prepared without adhesion exhibits an increasing probability x_i as the degree of freedom of the cell increases. Additionally, it is interesting to note that for such a packing, x_i is approximately proportional to the degree of freedom of the cell as conjectured in [35]. We observed however that the angles α, β, and γ are not evenly distributed in the $[\frac{\pi}{3},\frac{\pi}{2}]$ interval. Instead, and as already observed by Donev *et al.* [11], the angles show a divergence (maximum) close to $\frac{\pi}{3}$ with a minimum located close to $\frac{\pi}{2}$. The divergence at $\frac{\pi}{3}$ is of course related to the shape of the radial distribution function $g(r)$ close to $r=2R$ (Fig. 3).

Adhesion increases the probability of occurrence of fcc cells (as depicted graphically in Fig. 6) and of triclinic cells for which only one angle is not equal to $\pi/3$. Thus, there is a clear shift of the microstructure toward triclinic cells that exhibit lower degrees of freedom. The development of such localized dense cells is not accompanied by an increase in packing fraction. On the contrary, as pointed out in Sec. III, adhesion lowers the macroscopic packing fraction. This is because adhesion between particles hinders local rearrangements by introducing a critical tensile force for separation at contacts [Eq. (4)]. Friction has the opposite effect on the microstructure as compared to adhesion. Triclinic cells with three degrees of freedom are much more numerous as compared to the case without friction.

VII. CONCLUSIONS

In this study, the effect of adhesion and/or friction on the global and local geometry of monosized particle packing has been investigated. Some of the important observations are highlighted in this section. It is generally observed that an increase of ordering results in denser packings at the macroscopic level [5–7,9,10,36,37]. The simulations presented here, which use realistic elastic properties for adhesive particles, show that this may not always be the case. Indeed, when the ordering is triggered by adhesion at the scale of a few particles, it decreases the overall packing fraction. Such particle ordering is felt only at the very local level when adhesion plays a role in the packings studied here. This is likely the reason for the failure of the Q_6 order parameter to clearly detect some difference between adhesive and nonadhesive packings. It is interesting to note that the simple and venerable radial distribution function $g(r)$ is better suited to detect such localized ordering.

We believe that the classification that we have introduced, using four triclinic cells, offers a simple yet powerful tool to describe the existence of localized order (at the scale of a few particles). In particular, we have shown that, for packings that are not influenced by adhesion or friction, the probability of finding a given cell is approximately proportional to the degree of freedom of the cell. This shows that some localized order may be observed in so-called random close packings. Introducing adhesion increases the probability of occurrence of cells with lower degrees of freedom whereas friction has the reverse effect. Although adhesion and friction have opposite effects on the local microstructure of the packing, both interactions tend to lower the packing fraction at the macroscopic level.

Finally, we have shown here that the local microstructure of very stiff particle packings (typically ceramics) may also be affected by adhesion.

ACKNOWLEDGMENT

We would like to thank Aleksandar Donev from Lawrence Livermore National Laboratory for kindly providing the subroutine for calculating Q_6.

[1] J. D. Bernal and J. Mason, Nature (London) **188**, 910 (1960).
[2] *Disorder and Granular Media*, edited by D. Bideau and A. Hansen (Elsevier, Amsterdam, 1993).
[3] G. D. Scott, Nature (London) **188**, 908 (1960).
[4] S. Torquato, T. M. Truskett, and P. G. Debenedetti, Phys. Rev. Lett. **84**, 2064 (2000).
[5] P. Richard, L. Oger, J.-P. Troadec, and A. Gervois, Phys. Rev. E **60**, 4551 (1999).
[6] T. M. Truskett, S. Torquato, and P. G. Debenedetti, Phys. Rev. E **62**, 993 (2000).
[7] A. R. Kansal, S. Torquato, and F. H. Stillinger, Phys. Rev. E **66**, 041109 (2002).
[8] V. Luchnikov, A. Gervois, P. Richard, L. Oger, and J. P. Troadec, J. Mol. Liq. **96-97**, 185 (2002).
[9] C. S. O'Hern, L. E. Silbert, A. J. Liu, and S. R. Nagel, Phys. Rev. E **68**, 011306 (2003).

[10] K. Lochmann, A. Anikeenko, A. Elsner, N. Medvedev, and D. Stoyan, Eur. Phys. J. B **53**, 67 (2006).
[11] A. Donev, S. Torquato, and F. H. Stillinger, Phys. Rev. E **71**, 011105 (2005).
[12] F. Radjaï, M. Jean, J.-J. Moreau, and S. Roux, Phys. Rev. Lett. **77**, 274 (1996).
[13] C. Thornton and S. J. Antony, Proc. R. Soc. London, Ser. A **356**, 2763 (1998).
[14] H. A. Makse, D. L. Johnson, and L. M. Schwartz, Phys. Rev. Lett. **84**, 4160 (2000).
[15] L. E. Silbert, D. Ertas, G. S. Grest, T. C. Halsey, and D. Levine, Phys. Rev. E **65**, 031304 (2002).
[16] K. R. Shull, Mater. Sci. Eng., R. **36**, 1 (2002).
[17] F. A. Gilabert, J.-N. Roux, and A. Castellanos, Phys. Rev. E **75**, 011303 (2007).
[18] R. Y. Yang, R. P. Zou, and A. B. Yu, Phys. Rev. E **62**, 3900 (2000).
[19] R. Y. Yang, R. P. Zou, and A. B. Yu, J. Appl. Phys. **94**, 3025 (2003).
[20] D. E. Wolf, T. Unger, D. Kadau, and L. Brendel, in *Powders and Grains*, edited by R. G. Rojo, H. J. Herrmann, and S. McNamara (Balkema, Leiden, 2005), pp. 525–533.
[21] C. L. Martin, D. Bouvard, and S. Shima, J. Mech. Phys. Solids **51**, 667 (2003).
[22] K. L. Johnson, K. Kendall, and A. D. Roberts, Proc. R. Soc. London, Ser. A **324**, 301 (1971).
[23] B. Derjaguin, V. M. Muller, and Y. P. Toporov, J. Colloid Interface Sci. **53**, 314 (1975).
[24] J. A. Greenwood, Proc. R. Soc. London, Ser. A **453**, 1277 (1997).
[25] K. L. Johnson and J. A. Greenwood, J. Colloid Interface Sci. **192**, 326 (1997).
[26] K. L. Johnson, *Contact Mechanics* (Cambridge University Press, Cambridge, U.K., 1985).
[27] P. Dantu, Geotechnique **18**, 50 (1968).
[28] S. Torquato and F. H. Stillinger, J. Phys. Chem. B **105**, 11849 (2001).
[29] I. Agnolin and J.-N. Roux, Phys. Rev. E **76**, 061302 (2007).
[30] S. F. Edwards and D. V. Grinev, Phys. Rev. Lett. **82**, 5397 (1999).
[31] T. M. Truskett, S. Torquato, S. Sastry, P. G. Debenedetti, and F. H. Stillinger, Phys. Rev. E **58**, 3083 (1998).
[32] T. Aste, M. Saadatfar, and T. J. Senden, Phys. Rev. E **71**, 061302 (2005).
[33] M. A. Miller and D. Frenkel, J. Phys.: Condens. Matter **16**, S4901 (2004).
[34] P. J. Steinhardt, D. R. Nelson, and M. Ronchetti, Phys. Rev. B **28**, 784 (1983).
[35] R. K. Bordia, Scr. Metall. **18**, 725 (1984).
[36] I. Volkov, M. Cieplak, J. Koplik, and J. R. Banavar, Phys. Rev. E **66**, 061401 (2002).
[37] A. V. Anikeenko, N. N. Medvedev, A. Bezrukov, and D. Stoyan, J. Non-Cryst. Solids **353**, 3545 (2007).